Fermi National Accelerator Laboratory

FN-335
7420.180
March 1981

Risto Orava

Quark Jets

Operated by Universities Research Association Inc. under contract with the United States Department of Energy

TITLE: QUARK JETS

AUTHOR: Risto Orava
Fermi National Accelerator Laboratory,
Batavia, Illinois 60510, U.S.A., and
University of Helsinki,
Helsinki, Finland (SF), 1981

CLASSIFICATION: High Energy Physics

Abstract

We present evidence for "up"-("down"-) quark origin of the jets of hadrons observed in deep inelastic neutrino (antineutrino)-nucleon scattering and perform a systematic study of the structure of the jets.

By measuring ratios between the inclusive production rates of different mesons in the jets and by analyzing the jet net charge in detail, we provide evidence for the "up"-("down"-) quark fragmentation as the origin of hadrons observed in neutrino (antineutrino) -nucleon scattering. Good overall agreement with the simple quark-parton picture with universal fragmentation functions obeying isospin systematics is established.

We present evidence for scaling deviations in the quark fragmentation functions and evidence for a breakdown of the factorization hypothesis in the single particle inclusive cross section at small center-of-mass energies. Although the results are consistent with the leading order QCD predictions for the Q^2-dependence of the nonsinglet moments of the quark fragmentation functions, we point out that the observed Q^2-evolution is also expected to follow from an overlap between the target and

current fragmentation regions.

We use the ratio between the inclusive production rates of K^0- and π^--mesons in antineutrino-nucleon interactions to measure the size of SU(3) symmetry violation in the production of quark-antiquark pairs to be 0.27 ± 0.04.

By summing cumulatively electric charges of hadrons produced over the range of rapidities in antineutrino-nucleon charged current interactions, we show that the hypothesis of local charge conservation (LCC) is approximately valid above center-of-mass energies of 4 GeV. Charge compensation in the current fragmentation region seems to occur in a shorter rapidity interval than in proton-proton interactions at comparable center-of-mass energies.

Finally, we extend our systematic studies on the properties of hadron jets in antineutrino-nucleon charged current interactions to those observables which characterize the distribution of particles perpendicular to the jet axis. We find that these antineutrino induced jets have properties similar to those of the jets observed in e^+e^--annihilation at similar center-of-mass energies. We find no deviations from the simple quark-parton model. We also give an estimate for the quark "Fermi motion".

This paper summarizes the following publications on quark jets:

I Net Charge in Deep Inelastic Antineutrino-Nucleon Scattering, Physics Letters 91B (1980) 311, (with members of the FIIM Collaboration[1]).

II Quark Jets from Antineutrino Interactions I; Net Charge and Factorization in the Quark Jets, Fermilab-Pub-80/62-EXP(1980), to be published in Nuclear Physics B, (with members of the FIIM Collaboration[1]).

III Quark Jets from Antineutrino Interactions II; Inclusive Particle Spectra and Multiplicities in the Quark Jets, Fermilab-Pub-80/96-EXP(1980), to be published in Nuclear Physics B, (with members of the FIIM Collaboration[1]).

IV Observation of Scaling Deviations in the Energy Distribution of Secondary Hadrons in Inelastic Neutrino-Proton Interactions, Physics Letters 87B (1979) 281, (with members of the ABCMO Collaboration[2]).

V Measurement of SU(3) Symmetry Violation in the Quark Jet, Physics Letters 93B (1980) 210, (with members of the FIIM Collaboration[1]).

VI Charge Compensation in the Quark Jet, Fermilab-Pub-81/16-EXP(1981), submitted to Nuclear Physics B.

VII Quark Jets from Antineutrino Interactions III; Transverse Structure of the Quark Jets, Fermilab-Pub-81/30-EXP(1981), submitted to Nuclear Physics B,
(with members of the FIIM Collaboration[1]).

INTRODUCTION

Confined Quarks

Quarks still remain hypothetical "elementary particles" despite our intense research concentration on them. The quark hypothesis explains a multitude of phenomena such as hadron spectroscopy. Although we do not observe the quark directly, we are led to believe that it contributes to complex particle substructure. Our focus has therefore to be shifted to indirect ways of establishing the existence of quarks and to the problem of confinement, i.e., to the question: what is the mechanism that confines the quarks into the hadron states?

Hard Scattering Processes

A specific class of particle-particle collisions, called "hard scattering processes", is being used to test the idea of constituent quarks and to learn about the confining forces between the quarks. With a "hard" process, we mean a violently inelastic particle-particle collision that can be utilized to probe inner structure of the interacting particles. We define these hard scattering processes by Fig. 1, where each one of the described interactions involves a scattering of a pointlike probe off a pointlike constituent, e.g., quark, that is thought to be free at the time of interaction. This simple constituent model of the hadron and its interactions (Quark-Parton Model, QPM)[3,4] successfully describes numerous experimental results in the hard scattering processes. Experimental analysis identifies the constituents that interact with the probe as quarks with fractional electric charges.[5] To explain the

observed e^+e^--annihilation rate to hadrons (Fig. 1a), we need a new quark quantum number, color.[6] To explain deep inelastic lepton-nucleon scattering (Fig. 1b), we have to assume that about half of the nucleon momentum is carried by neutral constituents that do not couple to the lepton probes.[7]

Quantum ChromoDynamics

The theory called Quantum ChromoDynamics (QCD) incorporates the idea of colored quarks that are asymptotically free with the concept that neutral gluons mediate the colored strong coupling between quarks.[8] The simple QPM survives as a zero order approximation of the theory. Asymptotic freedom thus provides justification for the quark-parton picture although the QCD predictions differ from the simple QPM predictions due, for example, to the gluon bremsstrahlung process. The theory has not, however, provided a rigorous proof or description of quark confinement.

Deep Inelastic Scattering

In the QPM of deep inelastic lepton-nucleon scattering, we view a fast moving nucleon as a bag of structureless partons (hadron constituents) that all travel in the same direction as their bound state hadron (Fig. 2a). The partons share the nucleon momentum and appear to the incoming pointlike probe as free objects inside the rapidly moving nucleon. We obtain the reaction rate as an incoherent sum over all contributing pointlike interactions that are described as mediated by a "current". The electromagnetic current carries the quantum numbers of the photon and couples to each kind of quark (quark flavors) with strength that is proportional to the squared electric charge of the quark. The "weak" charged current that

is carried by the hypothetical W-bosons, on the other hand, should effectively couple to one particular kind of quark in the nucleon. Neutrino (antineutrino) interactions, that are mediated by the weak charged current, should then be dominated by pointlike current-"down" quark (current-"up" quark) interactions and thus provide a unique testing ground of the basic QPM ideas.

Quark Fragmentation

It is conjectured that in a time scale long compared to the "instantaneous" current-quark interaction the quark struck by the current converts or "fragments" into the observed final state hadrons (Fig. 2b).[3,9] The hadrons have their inclusive spectrum independent of the initial state (Universality) and the spectrum is determined by the fragmenting quark and by z, the fraction of the quark momentum carried by a hadron h (Scaling).

Two characteristic features of hadron fragmentation in high energy hadron-hadron collisions are (1) the existence of a flat plateau in rapidity, i.e., the product particle distribution is constant in rapidity, (the rapidity variable is a scaled particle velocity that has convenient properties under Lorentz transformation); and (2) the retention of hadron quantum numbers, on the average, in the hadron fragmentation region (in the ends of the rapidity distribution). Berman, Bjorken, and Kogut have argued that parton fragmentation should also develop a rapidity plateau[10] and Feynman has suggested that the quantum numbers of the quark-parton are also retained, on the average, in the quark fragmentation region.[3] Several phenomenological models for the "soft" processes that describe how quarks (and gluons) fragment into the hadron states and that incorporate the idea of rapidity plateau and the idea of quark quantum

number retention have been proposed.

QCD and Parton Fragmentation Functions

Varying the lepton four-momentum transfer squared, Q^2, we vary the distance scale that we are probing in our experiment. The larger Q^2 the smaller the details we shall resolve in our sample. The Q^2-evolution of the parton fragmentation functions, calculated in leading order perturbative QCD (applicable when the strong coupling is small enough to be considered as a perturbation), is determined by a recursion relation between the fragmentation function at one scale and that at another scale. Physical interpretation is provided by Kogut and Susskind[11] who describe the hadrons as being made up of infinite levels of partons that, when probed by a virtual probe with mass squared equal to Q^2, reveal constituents with the size scale of $1/Q$. Uematsu uses a modification of the Kogut-Susskind recursion relation, so called Altarelli-Parisi equation, to set up integral equations for the Q^2 development of the parton fragmentation functions.[12]

Recent studies in QCD perturbation theory[13] show that one may not talk of universal Q^2-dependent fragmentation functions if the next to the leading order effects are accounted for. Predictions for violation of the factorization hypothesis follow from these calculations.

QCD perturbation theory gives predictions for the Q^2-evolution of the parton fragmentation functions and for factorization violation of the single particle inclusive cross section. At our relatively low energies the "soft" confinement processes still dominate, however, and phenomenological models are needed to describe quark and gluon fragmentation.

It is our purpose in this work to provide evidence for confined quarks in final states in deep inelastic lepton-nucleon scattering and to present a detailed description of the structure of the jets of hadrons that are produced as a consequence of quark confinement.

Experiments

In our experimental analysis we use data from an anti-neutrino-nucleon experiment in the Fermilab 15-foot bubble chamber[14] equipped with the Fermilab External Muon Identifier (EMI)[15] (Fig. 3) and from a neutrino-hydrogen experiment in the Big European Bubble Chamber (BEBC)[16] equipped with the CERN (Conseil Européen pour la Recherche Nucléaire) EMI.[17]

Fermilab 15-Foot Bubble Chamber

The Fermilab 15-foot bubble chamber has been constructed from spherical shapes to reduce the thickness of the walls of the chamber body and the surrounding vacuum tank. Three of the six cameras on top of the chamber are used. The cameras have fisheye optics with 108^{0} lenses and 70mm film. The inner surface of the bubble chamber is covered with Scotchlite which, as a retrodirective material, reflects the light emitted by the flashtubes back to the cameras. The large superconducting magnet surrounds the chamber and produces a magnetic field of 30kG at the center of the chamber. The shape of the chamber is roughly spherical with a diameter of 12.5 feet and with a conical "nose" in the upstream direction. The total length of the chamber, measured along the antineutrino beam direction is 15 feet. The chamber can be filled to a useful volume of 1 ton hydrogen, 2 tons of deuterium, or 20 tons of neon. The piston is fiberglass (six feet in diameter) with pressure assisted lip seal rings. Around the chamber on the downstream direction is situated the Fermilab EMI.

Fermilab EMI

The Fermilab EMI consists of 3-5 interaction lengths of absorber followed by an array of 24 Multiwire Proportional Wire Chambers (MPWC's)

each with an area of 1 m^2. The EMI extends about 45^o vertically and 135^o horizontally as seen from the center of the chamber. All tracks that are left by the final state particles in the bubble chamber are measured and tracks that do not undergo interactions in the chamber are extrapolated to the plane of the proportional chambers. Due to the measurement errors and multiple Coulomb scattering in the absorber, an ellipse, rather than a point specifies the location where a "hit" in the EMI would be expected if the extrapolated track were indeed a muon. Final state hadrons almost invariably interact and scatter before reaching the EMI. Taking into account background hits and chamber inefficiencies, we assign confidence levels that a track is a muon or a hadron.

BEBC and BEBC EMI

The liquid volume of the BEBC, $32m^3$, is basically a cylinder 3.5 m in diameter and 4 m in height. The visible volume is about $20m^3$ with a useful volume of about $10m^3$. The chamber is surrounded by a superconducting magnet which produces a field of 30kG. The magnetic return path is an iron cylinder 12m in diameter. Three types of fillings can be used as in the case of the Fermilab 15-foot bubble chamber: (a) 0.75 tons of hydrogen, (b) 1.5 tons of deuterium, or (c) 10 tons of neon. Downstream of the BEBC is situated the BEBC EMI of $15m^2$ area of MWPC's. The BEBC EMI is similar to the Fermilab EMI.

Beams

Our antineutrino data come from the exposures of the Fermilab 15-foot bubble chamber to a wide-band double horn focussed antineutrino beam[18] and, in the second run to a Bare Target Sign Selected (BTSS) antineutrino

beam[19] (Table 1).

We show the layout of the Fermilab neutrino area in Fig. 4. Protons extracted from the main ring of the accelerator interact in an aluminum target and produce mainly pions and kaons. The subsequent decays of the pions and kaons produce the antineutrinos (and neutrinos) that are utilized in our experiments (Table 2).

For the first run with the Fermilab 15-foot bubble chamber, a double horn that produces a toroidal magnetic field was used as a focussing device (Fig. 5a). The double horn consists of two concentric conical conductors made from aluminum and it carries a pulsed current of about 350kA. The target was positioned lengthwise along the beam direction in the neck of the double horn. The shape of the horn was designed so as to defocus positively charged mesons. Since the horn does not affect positively charged high energy hadrons traversing the center of the horn, an absorbtive plug was placed downstream of the target. The plug reduces the high energy neutrino and antineutrino flux.

The BTSS antineutrino beam was used in the second run with the Fermilab 15-foot bubble chamber. The BTSS beam consists of a pair of dipole magnets which select the charge of the desired particles (Fig. 5b). The particles with the opposite charge are stopped in a beam dump. After leaving the hadron selection area, the particles enter a 400m drift space. A fraction of the pions and kaons decay into neutrinos (antineutrinos) through the decay modes listed in Table 2 (Ref. 20). An earth and iron shield of approximately 1000m follows the decay region. Hadrons interact soon after entering the shield while muons only slowly loose their energy by ionization. At the end of the shield almost all of the muons have been

"ranged out" so that an almost pure beam of antineutrinos (neutrinos in the BEBC experiment) is left to enter the bubble chamber. Background from neutrinos and neutral hadrons is present due to neutrino-interactions in the shield and in the exterior of the bubble chamber.

We obtained the neutrino-hydrogen data by using the CERN double-horn focussed wide-band neutrino beam[21] that differs from the Fermilab double-horn focussed wide-band beam by some design parameters that are immaterial for this description.

Data Processing

The antineutrino (neutrino) experiment with the Fermilab 15-foot bubble chamber (with BEBC) resulted in about 180,000 (285,000) photographs. Each picture was first double-scanned for interactions induced by neutral particles in the chamber volume. The scanning was performed by specially trained personnel in each collaborating laboratory according to a set of scanning rules set by the collaboration. The results were checked in a third scan by physicists belonging to the collaboration. A partial rescan of the events gives for the overall scan efficiency of the Fermilab anti-neutrino-nucleon events (of the BEBC neutrino-hydrogen events) 94% (99%).

All the antineutrino (neutrino) events were then digitized and recorded on magnetic tapes by automatic and/or semi-automatic film processing devices in the collaborating laboratories. Secondary neutral particle interactions, photon conversions to electron-positron pairs and neutral strange particle decays were measured along with the primary tracks in the events. Tracks emerging from the secondary interactions on the charged primary tracks were measured whenever they provided potential

improvement in the measurement of the primary track momentum. The resulting magnetic tape was used as an input to a chain of data processing programs and the measured events were finally reconstructed by a CERN HYDRA geometry program.[22] Kinematical fits to various exclusive final states were tried for the neutrino-hydrogen events (BEBC) and about 10% of the events gave a satisfactory fit to one or several different channels.

The residual error, that represents the r.m.s scatter of measured points about the fitted track, of the measuring devices peaks at about 10 μm on film. Events which fail geometry tests are remeasured as many times as necessary for a successful event reconstruction. Event records are then edited and merged together with the EMI records. The final result, the Data Exchange Tape (DET) is distributed to all collaborating laboratories.

Data Samples

We obtained the antineutrino-nucleon charged current event sample of the type $\bar{\nu}_\mu N \to \mu^+ + \text{hadrons}$ in the Fermilab 15-foot bubble chamber filled with a neon-hydrogen mixture of 64% atomic neon and it consists of 7200 events in which we require the final state muons to have their laboratory momenta larger than 4 GeV/c and to be identified by the Fermilab EMI supplemented by a large transverse momentum procedure.[23] The antineutrino energy in these events ranges from 7.5 GeV to 200 GeV with the energy distribution peaking at 18 GeV. The neutrino component in our antineutrino event sample is about 15% averaged over the antineutrino energy spectrum for antineutrino energy $E_{\bar{\nu}} > 10$ GeV. We use also our neutrino event sample of 1100 charged current events obtained in the Fermilab 15-foot bubble chamber in our

analysis. This event sample fulfills the same selection criteria as the Fermilab $\bar{\nu}_\mu N$ event sample.

The neutrino-hydrogen event sample consists of 5600 charged current events of the type $\nu_\mu p \rightarrow \mu^- +$hadrons where the final state muons are required to have their laboratory momenta larger than 3 GeV/c and to be identified by the CERN EMI. The neutrino energies in these events range from 5 GeV to 200 GeV with the energy distribution peaking at about 25 GeV.

SUMMARY OF PAPERS

Paper I

In Paper I we present the first systematical measurement on the net electric charge of hadrons produced in charged current antineutrino-nucleon (neutrino-nucleon) interactions of the type $\bar{\nu}_\mu N \to \mu^+ + \text{hadrons}$ ($\nu_\mu N \to \mu^- + \text{hadrons}$). Extrapolation of the average net charge, measured as a function of the center-of-mass energy, W, to infinite W gives the result of -0.44 ± 0.09 ($+0.54 \pm 0.12$) for the antineutrino (neutrino) induced hadron jets (Fig. 6). Within the framework of the simple QPM this result identifies the flavor of the scattered quark to be "down" ("up") in antineutrino (neutrino) charged current interactions. We interpret the result according to the simple QPM and obtain for the relative probability of creating a new "down"-"antidown" or "up"-"antiup" quark-antiquark pair in the quark fragmentation process the result 0.44 ± 0.09.

In Paper I we also point out that the net charge of the jet does not measure the electric charge of the scattered quark as was originally argued.[3]

Finally, in Paper I we measure the so called "weighted charge" distribution for hadrons produced in antineutrino-nucleon charged current interactions and find that the results are consistent with the predictions for "down"-quark fragmentation. The results are not consistent with the predictions for "up"-quark fragmentation[24] (Fig. 7a,b).

Paper II

In Paper II we systematically extend our analysis on the net charge of the jet produced in charged current antineutrino (neutrino) interactions. Results consistent with the simple QPM predictions[24] emerge for both antineutrino and neutrino interactions.

Our measurement of the weighted charge distributions in the neutrino induced jets gives results that are consistent with the QPM prediction for "up"-quark fragmentation but that are not consistent with the predictions for the "down"-quark fragmentation[24] (Fig. 7c,d).

We measure Bjorken-x and squared lepton four-momentum transfer, $-q^2$, dependences of the average net charge of the jet and the average weighted charge in the antineutrino induced jets. Qualitative support is found for the presence of antiquarks among the scattered fragmenting partons.

In Paper II we perform the first direct test of the factorization hypothesis[3] for the single-particle inclusive cross section in antineutrino interactions. We find no significant violation of the hypothesis that the fragmentation functions are independent of the initial state.

Finally, in Paper II we discuss and measure various experimental uncertainties that are present in the analysis. We compare our results with Monte Carlo model calculations. This comparison includes our measurement systematics and antineutrino beam spectrum but does not include any built-in particle-particle correlations, except those induced by a parametrization of the observed average charged particle multiplicity as a function of W. We note that our results for the average jet net charge have important consequences in tests of QCD.

Paper III

After having established in Paper II the approximate validity of the factorization hypothesis, we investigate in Paper III the quark fragmentation functions $D_q^h(z)$. These functions describe the probability that a quark q will fragment to a hadron h with fraction z of the quark momentum. We compare our results with the results obtained in other hard scattering (at different c.m.s energies) processes[25] and find support for the concept of Universality and Scaling of the quark fragmentation functions by observing good agreement between the different fragmentation function measurements (Fig. 8).

We test the validity of relations that follow from isospin symmetry and isospin conservation between the quark fragmentation functions[24] and find good overall agreement with the expectations of the simple QPM.

Our measurement of the ration $D_q^{h^-}(z)/D_q^{h^+}(z)$, where h^+ and h^- are positively and negatively charged final state mesons in reactions $\bar{\nu}_\mu N \to \mu^+ +$hadrons, provides additional evidence for the "down"-quark origin of the hadrons in the antineutrino charged current induced jets (Fig. 9). The evidence is based on the expectation that there is no positively charged particles at the limit $z \to 1$.

In our analysis we perform the first measurement of proton contamination in the fragmentation function of "down"-quark into positively charged mesons by measuring for a "down"-quark fragmentation probability to the lambda-hyperons observed in our experiment. In our measurements, we also carefully account for the "smearing" effects that always appear in the measured inclusive spectra due to the experimental uncertainties and limited acceptance.

In Paper III we also study charged particle multiplicities in the antineutrino charged current induced jets. We find that the hadron multiplicities are of the same order of magnitude as in the hadron jets observed in e^+e^- -annihilation process.[26] We provide convenient parametrizations for the jet multiplicities that may be used for predictions of the jet properties at higher energies.

Paper IV

In Paper IV we search for deviations from predictions of the simple QPM for the quark fragmentation functions. We compare the $-q^2$ -evolution of moments of the fragmentation functions to the leading order calculations in perturbative QCD.[11] We report qualitative agreement with the QCD predictions.

We observe that both the measured $-q^2$ -dependence of the fragmentation function moments and apparent violation of the factorization hypothesis are confined to small center-of-mass energies ($W \leq 4$GeV). Our investigation of the jet net charge in Papers I and II show that there is a significant overlap between the "target" and "current" fragmentation regions at small c.m.s energies ($W \leq 4$GeV) and that the overlap diminishes with increasing W. Due to the correlation between the variables W,$-q^2$ and Bjorken-x a $-q^2$ dependence and a factorization violation that diminishes as W increases is then expected to occur for the quark fragmentation functions. Here one has to make a distinction between the perturbative QCD effects that involve hard gluon bremmstrahlung from the outgoing quark and the "soft" particle production processes that give rise to the overlap (see Fig. 10).

Paper V

We base our Paper V on the results that we report in Papers I-III and assume that the fragmenting quark in charged current antineutrino interactions is a "down"-quark. We then measure the ration, p_s/p, between the probabilities of producing a "strange-antistrange" (p_s) and "up-antiup" (p) quark-antiquark pair in the quark jets originated by the "down"-quarks. In the perfectly SU(3) symmetric case, the ratio p_s/p would be equal to one. We obtain the result $p_s/p=0.27\pm0.04$ for the SU(3) symmetry violation by investigating the relative production rates of K^o-mesons and negatively charged mesons as a function of the fractional momentum, z, in the jets produced in our sample of charged current antineutrino events (Fig. 11). Our result indicates significantly stronger suppression of "strange" quarks than the previously accepted value of 0.5 for the ratio p_s/p.[24]

Paper VI

We analyze in Paper VI how the electric charge of hadrons in the jets is "neutralized" or compensated locally. This is the first measurement in lepton produced jets.

The hypothesis of Local Compensation of Charge (LCC) is a consequence of quark fragmentation models that assume dominantly short range correlations amongst the final state particles.[27]

In this Paper we demonstrate that the region of overlap between the "target" and "current" fragmentation regions has a significant impact upon the so called rapidity zone distribution that we use in Paper VI to measure the average rapidity interval required for charge compensation in the jets (Fig. 12). We find that the LCC hypothesis is approximately valid in our

antineutrino charged current induced jets above 4 GeV in c.m.s energy. We measure the average rapidity interval required for charge compensation, $\langle\lambda_o\rangle$, and find $\langle\lambda_o\rangle=0.57\pm0.01$ that is about 20% smaller than the results obtained in proton-proton experiments at comparable c.m.s energies.[28]

Paper VII

In Paper VII we systematically extend our studies on the properties of hadron jets produced in antineutrino-nucleon charged current interactions to those observables that characterize the distribution of particles perpendicular to the jet axis.

We find that these antineutrino charged current induced jets have properties similar to those of the jets observed in e^+e^- -annihilation to hadrons at comparable c.m.s energies[29] (Fig. 13).

We show that there is significant uncertainty in the definition of the jet axis at c.m.s energies of 4 GeV and below.

Contrary to previous experiments, we do not find any significant deviations from the simple QPM predictions in our systematic analysis.

ACKNOWLEDGEMENTS

I feel deep gratitude to the people who have provided me with their advice and support during the course of this work. I wish to thank Hannu I. Miettinen, Frank Nezrick, J. D. Bjorken, N. Brodsky, A. Buras, D. Cundy, R. P. Feynman, R. D. Field, K. Kajantie, K. Lassila, K. V. Laurikainen, D. R. O. Morrison, M. Roos, and J. Tuominiemi.

I am grateful to my colleagues in the FIIM Group[1] and in the ABCMO Group[2] for their collaboration, to the Fermilab and CERN bubble chamber crews, to the scanning and secretarial staffs at each respective laboratory for their excellent performance.

I also want to thank G. Stazak for carefully typing this report and E. Luisada for skillfully drawing the numerous figures in this work.

Finally, I want to express my gratitude to my wife, Kirsti, who (with my son, Samuli) has been a continuous source of encouragement and inspiration for the three years I have spent preparing this work.

REFERENCES

[1]Members of the Fermilab-IHEP-ITEP-Michigan University Collaboration: J.P.Berge, D.Bogert, R.Endorf, R.Hanft, J.A.Malko, G.I.Moffat, F.A.Nezrick, R.Orava and J.Wolfson(Fermilab); V.V.Ammosov, A.G.Denisov, G.S.Gapienko, V.A.Gapienko, V.I.Klukhin, V.I.Koreshev, P.V.Pitukhin, V.I.Sirotenko, E.A.Slobodyuk, Z.V.Usubov, and V.G.Zaetz (IHEP, Serpukhov); V.I.Efremenko, A.V.Fedotov, P.A.Gorichev, V.S.Kaftanov, G.K.Kliger, V.Z.Kolganov, S.P.Krutchinin, M.A.Kubantsev, I.V.Makhljueva, V.I.Shekeljan, and V.G.Shevchenko (ITEP, Moscow); J.Bell, C.T.Coffin, B.P.Roe, A.A.Seidl, D.Sinclair, and E.Wang (Michigan University).

[2]Members of the Aachen-Bonn-CERN-Munich(MPI)-Oxford Collaboration: J.Blietschau, H.Grässler, W.Krenz, D.Lanske, R.Schulte and H.H.Seyfert (Aachen); K.Böckmann, P.Checchia, C.Geich-Gimbel, H.Heilmann, T.Kokott, P.Nellen and R.Pech (Bonn); L.Bacci, P.Bosetti, D.C.Cundy, A.Grant, P.O.Hulth, D.R.O.Morrison, R.Orava, L.Pape, Ch. Peyrou, H.Saarikko, W.G.Scott, E.Simopoulou, A.Vayaki and H.Wachsmuth (CERN); M.Aderholz, N.Schmitz, R.Settles, K.L.Wernhard, and W.Wittek (Munich,MPI); R.Giles, P.Grossmann, R.McGow, G.Myatt, D.H.Perkins, D.Radojicic, P.Renton, and B.Saitta (Oxford).

[3]R.P.Feynman, Photon-Hadron Interactions (W.A.Benjamin, New York, 1972).

[4]J.D.Bjorken, Proceedings of 3rd International Symposium on Electron and Photon Interactions, Stanford, California (1967).
R.P.Feynman, Phys. Rev. Lett. 23(1969)1415.
J.D.Bjorken and E.A.Paschos, Phys. Rev. 185(1969)1975.
S.D.Drell and T.M.Yan, Phys. Rev. Lett. 25(1970)316.

[5]T.Eichten et al., Phys. Lett. 46B(1973)274.
H.Deden et al., Nucl. Phys. B85(1975)269.

[6]See for example: F.Close, An Introduction to Quarks and Partons, Academic Press (London, 1979).

[7]P.C.Bosetti et al., Nucl. Phys. B142(1978)1.

[8]D.J.Gross and F.Wilczek, Phys. Rev. Lett 30(1973)1343.
H.D.Politzer, Phys. Rev. Lett. 30(1973)1346.
H.Fritzsch, M.Gell-Mann, and H.Leutwyler, Phys. Lett. 47B(1973)365.

[9]J.D.Bjorken, "Current Induced Reactions", Lecture Notes in Physics 56, Ed. J.G.Körner et al. (Springer-Verlag, 1976)93.

[10]S.M.Berman, J.D.Bjorken and J.B.Kogut, Phys. Rev. D4(1971)3338.

[11]J.B.Kogut and L.Susskind, Phys. Rep. 8C(1973)75.

[12]T.Uematsu, Phys. Lett. 79B(1978)97.
J.F.Owens, Phys. Lett. 76B(1978)85.

[13]N.Sakai, Phys. Lett. 85B(1979)67.

[14]Fermilab 15-Foot Bubble Chamber Safety Report, Ed. R.R.Huson, vols. I-III (1972), unpublished.

[15]R.J.Cence et al., Nucl. Inst. and Methods 138(1976)245.

[16]BEBC Users Handbook, CERN(1978).

[17]A.Grant, Construction of an EMI for BEBC, CERN-D.P h. II 73-2.

[18]F.Nezrick, IEEE Transactions on Nuclear Sciences, Vol. NS-22 (1975)1479.

[19]A.Benvenuti et al., Proceedings of the International Conference on High Energy Neutrino Physics, Paris (1975).

[20]Particle Data Group, N.Barash-Schmidt et al., Rev. Mod. Phys. 52, No. 2, Part II(1980).

[21]W.A.Venus and H.W.Wachsmuth, CERN Report RL-73-137(1973), unpublished.

[22]CERN HYDRA Application Library Long Write-Ups with modifications by J.P.Berge (Fermilab).

[23]The large transverse momentum procedure for muon identification is described in Paper II.

[24]R.D.Field and R.P.Feynman, Nucl. Phys. B136(1978)1.

[25]T.P.McPharlin et al., Phys. Lett. 90B(1980)479.
M.Basile et al., Phys. Lett. 45B(1980)5.

[26]R.Brandelik et al., Phys. Lett. 89B(1980)418.
G.Wolf, Rapporteur talk at the 1979 EPS International Conference on High Energy Physics, Geneva (1979).

[27]A.Krzywicki and D.Weingarten, Phys. Lett. 50B(1974)265.

[28]C.Bromberg et al., Phys. Rev. D12(1975)1224.
J.Derre et al., Local Compensation of Charge and Charge Transfer in pp Interactions at 69 GeV/c, a contribution to the Conference on High Energy Physics, London (1974).

[29]Ch. Berger et al., Phys. Lett. 78B(1978)176.

Table 1. Summary of the Exposures

Exposure	Fermilab 15-Foot No. 1	Fermilab 15-Foot No. 2	BEBC
Date	Winter-77	Spring-77	Autumn-77
No. of Pictures	88,700	96,200	285,000
Proton Energy	400 GeV	400 GeV	350 GeV
Avg. Proton Intensity	1.0 10^{13} ppp	1.4 10^{13} ppp	1.1 10^{18} ppp
Focusing Device	Double Horn	Two Dipoles BTSS	Double Horn
Chamber Filling	64% Ne/H_2	64% Ne/H_2	H_2

Table 2. Pion and Kaon Decay Modes to Neutrinos.[20]

Decay Mode	Branching Ratio
$\pi^- \rightarrow \mu^- \bar{\nu}_\mu$ $(\pi^+ \rightarrow \mu^+ \nu)$	~100%
$K^- \rightarrow \mu^- \bar{\nu}_\mu$ $(K^+ \rightarrow \mu^+ \nu)$	63.5%
$K^- \rightarrow \mu^- \pi^0 \bar{\nu}_\mu$ $(K^+ \rightarrow \mu^+ \pi^0 \nu_\mu)$	3.2%
$K^- \rightarrow e^- \pi^0 \bar{\nu}_e$ $(K^+ \rightarrow e^+ \pi^0 \nu_e)$	4.8%

FIGURE CAPTIONS

Fig. 1 Illustration of the "hard" scattering processes and their description in the simple Quark-Parton Model: (a) e^+e^- -annihilation to hadrons and the creation of a parton-antiparton pair (p-$\bar{p}$) in e^+e^- -annihilation, (b) deep inelastic lepton-nucleon scattering and absorption of the intermediate current by a free parton p, and (c) muon pair creation in nucleon-nucleon (N_1+N_2) collision and the corresponding process in QPM.

Fig. 2 Deep inelastic lepton-nucleon scattering in the simple Quark-Parton Model: (a) the intermediate current is absorbed by a free parton that scatters out from the nucleon. Cross section for the process can be expressed in terms of the parton density distributions $F_i(x)$ (x is the Bjorken-x variable) inside the target nucleon, (b) new parton-antiparton pairs appear between the scattered parton and the rest of the nucleon constituents. The new parton-antiparton pairs subsequently combine into the observed hadron states. Fragmentation probability of parton i to hadron h in the final state is described by the fragmentation function $D_i^h(z)$, where z is the momentum fraction carried by the hadron h.

Fig. 3 Top and side views of the Fermilab 15-foot bubble chamber equipped with the Fermilab External Muon Identifier.[14] A neutrino-proton charged current event of the type $\nu_\mu p \to \mu^-$ +hadrons is shown to occur in the bubble chamber.

Fig. 4 Layout of the Fermilab accelerator and the experimental areas.

Fig. 5 Layout of the neutrino area at Fermilab with (a) a layout of the double-horn focussed wide-band antineutrino beam, and (b) a layout of the Bare Target Sign Selected beam.

Fig. 6 Average net charge of the hadrons traveling forward in the hadronic center-of-mass system as a function of 1/W. The dashed line represents a linear fit to the data points above W=3GeV. The shaded area is a prediction from the Monte Carlo model that does not include the hypothesis of quark fragmentation (from Paper I).

Fig. 7 Weighted charge $Q_W^{\bar{\nu}} = \Sigma_i z_i^r e_i \ (Q_W^{\nu})$, where e_i is electric charge of i^{th} hadron, for antineutrino (neutrino) charged current induced hadrons traveling forward in the hadronic center-of-mass system (a,c) for r=0.2, and (b,d) for r=0.5. The solid curves represent the Field and Feynman predictions for the hadrons arising from the fragmentation of a u-quark with 10 GeV/c incident momentum and the dashed lines the corresponding predictions for the 10 GeV/c d-quark jets[24] (from Paper III).

Fig. 8 Fragmentation function $D^{h^{\pm}}(z)$ for charged hadrons traveling forward in the hadronic c.m.s in this experiment, in an ep-experiment;[25] in a proton-proton experiment,[25] and fragmentation function $D^{h^0}(z)$ for neutral pions in the ep-experiment[25]. The solid line represents a parametrization by Field and Feynman[24] with 0.27 as the magnitude of SU(3) symmetry violation (from Paper III).

Fig. 9 The ratio of negatively to positively charged hadrons $h^-/h^+ = D^{h^-}(z)/D^{h^+}(z)$ as a function of z for the charged hadrons traveling forward in the hadronic c.m.s in this experiment. The solid line represents a parametrization of Field and Feynman[24] in which the size of SU(3) symmetry violation is taken to be equal to 0.27 (from Paper III).

Fig. 10 The third moment of the u-quark fragmentation function to positively charged mesons $D^+(3,Q^2) = \int z^2 D^{h^+}(z,Q^2)dz$ as a function of lepton four-momentum transfer squared, Q^2, for two different c.m.s energy intervals (from Paper IV).

Fig. 11 The K^n/h^- ratio in the region $z_{min} < z < 1$ as a function of the lower limit, z_{min}. The cascade model calculation[24] for different values of SU(3) symmetry violation, p_s/p, are shown by solid curves (Paper V).

Fig. 12 (a) Average rapidity range required for charge compensation in the quark jets, $\langle \lambda_o \rangle$, as a function of the c.m.s energy for two different definitions of the "forward" rapidity zones.
(b) Average charged particle multiplicity in a rapidity zone $\langle n_z \rangle$ as a function of the c.m.s energy for two definitions of the "forward" rapidity zones. Open circles represent proton-proton results for central rapidity zones[28] (from Paper VI).

Fig. 13 Average transverse momentum squared of the charged hadrons in the "current" fragmentation region relative to the thrust axis, $\langle p_T^2 \rangle$, and relative to the $\mu\nu$-plane, $\langle p_{out}^2 \rangle$, as functions of W. Data from an e^+e^- -experiment are also shown[29]. The solid curves represent our Monte Carlo calculations with a LPS model (from Paper VII).

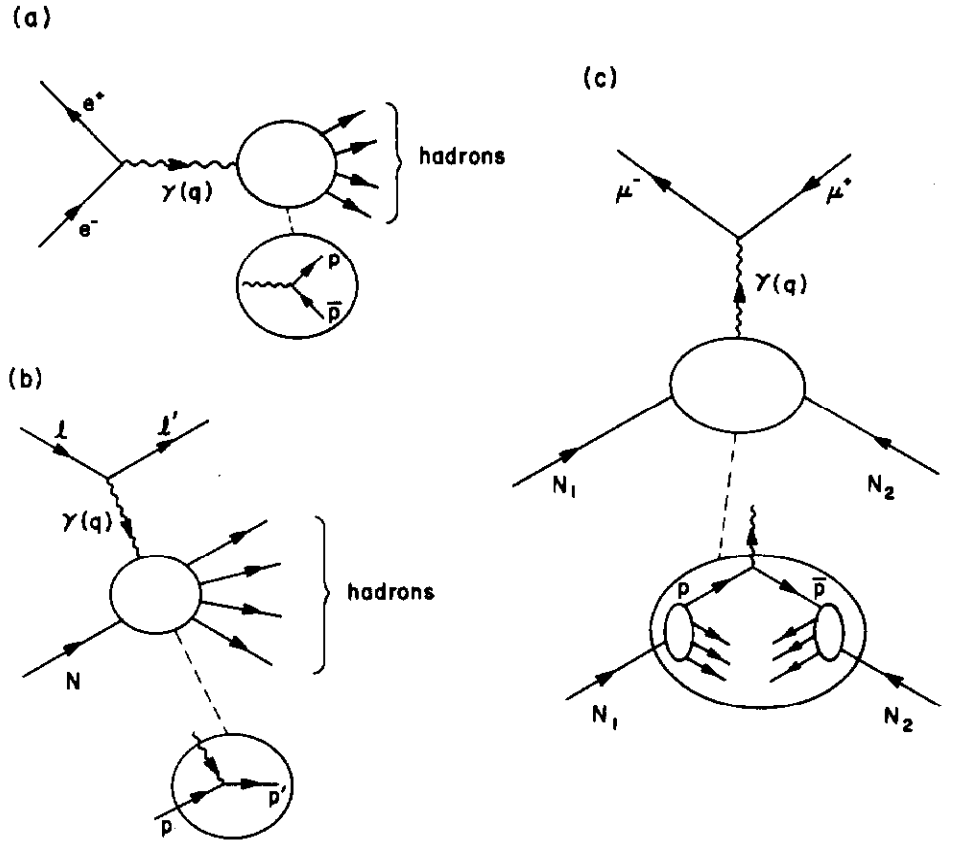

Fig. 1.

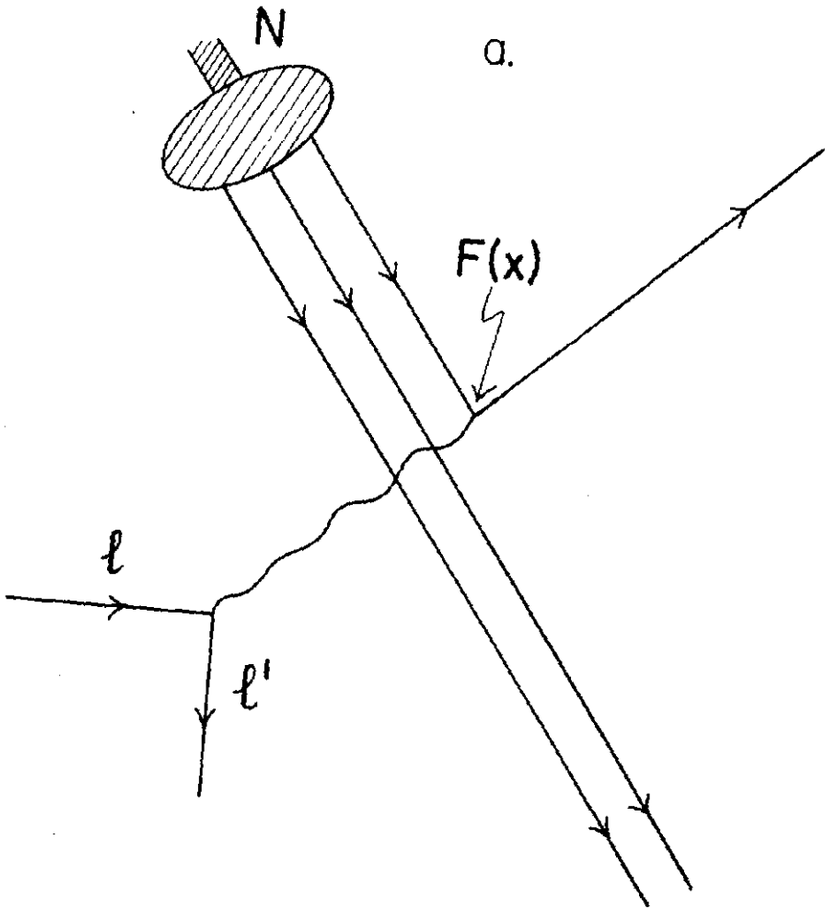

Fig. 2a.

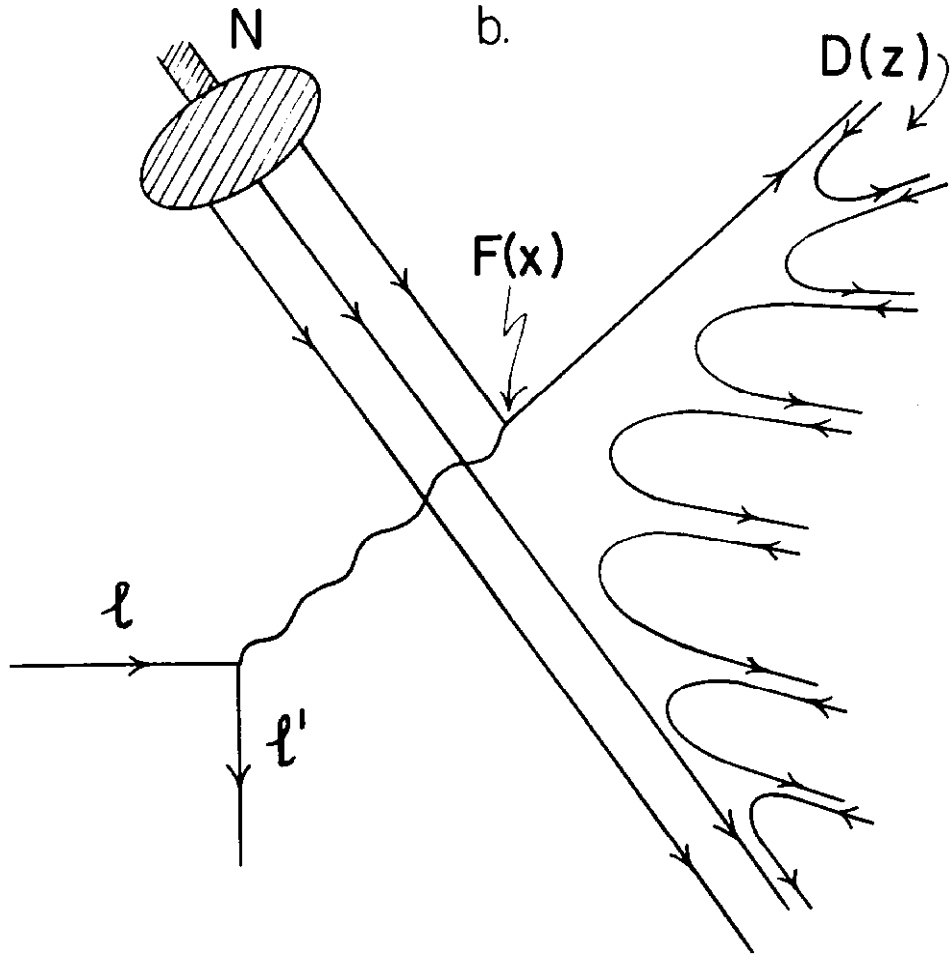

Fig. 2b.

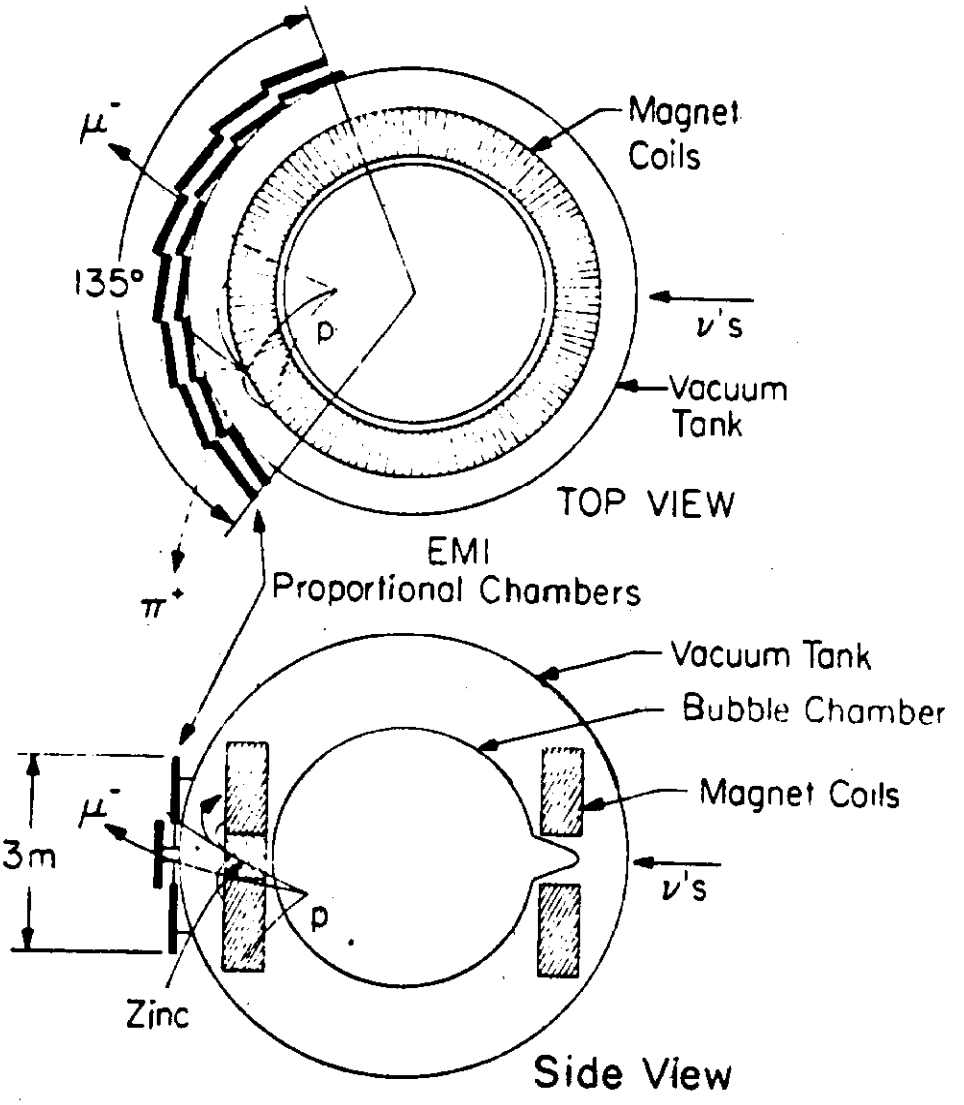
μ⁻
135°
Magnet Coils
p
ν's
Vacuum Tank
TOP VIEW
EMI
Proportional Chambers
π⁺
Vacuum Tank
Bubble Chamber
Magnet Coils
μ⁻
3m
ν's
p
Zinc
Side View

Fig. 3.

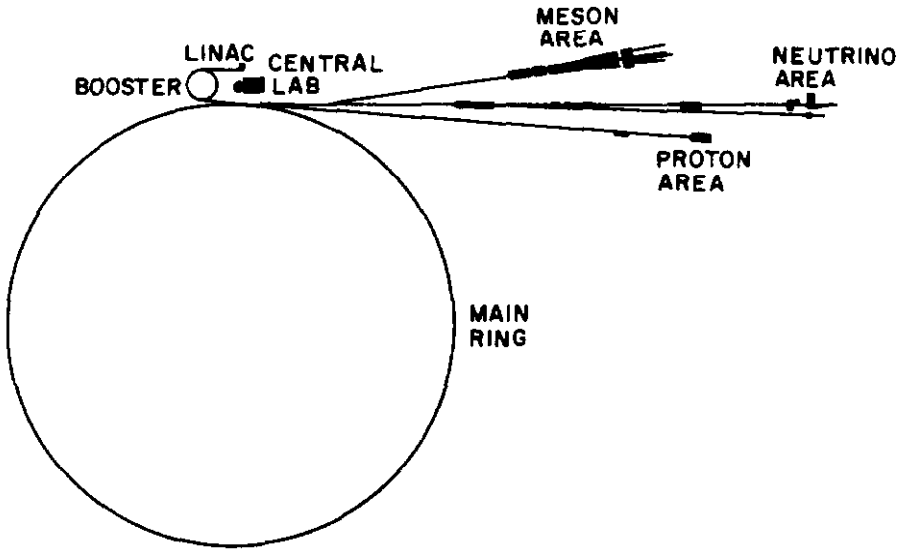

Fig. 4.

(a) DOUBLE HORN FOCUSED BEAM

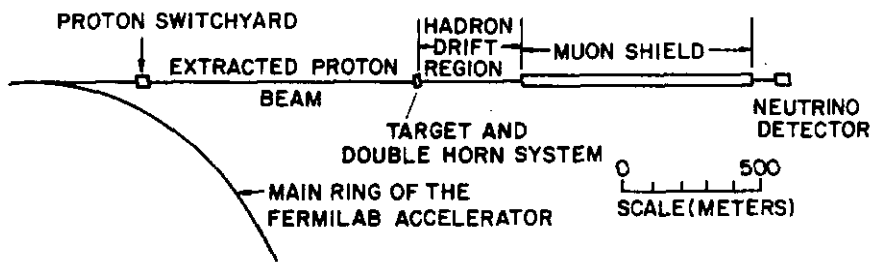

(b) BARE TARGET SIGN SELECTED BEAM

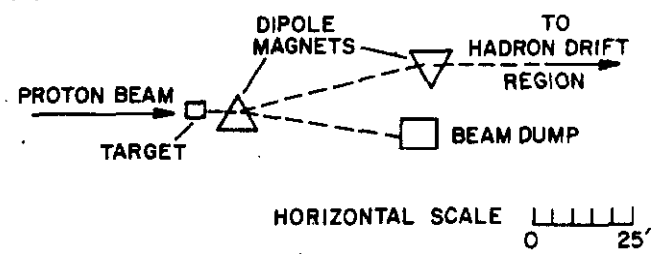

Fig. 5.

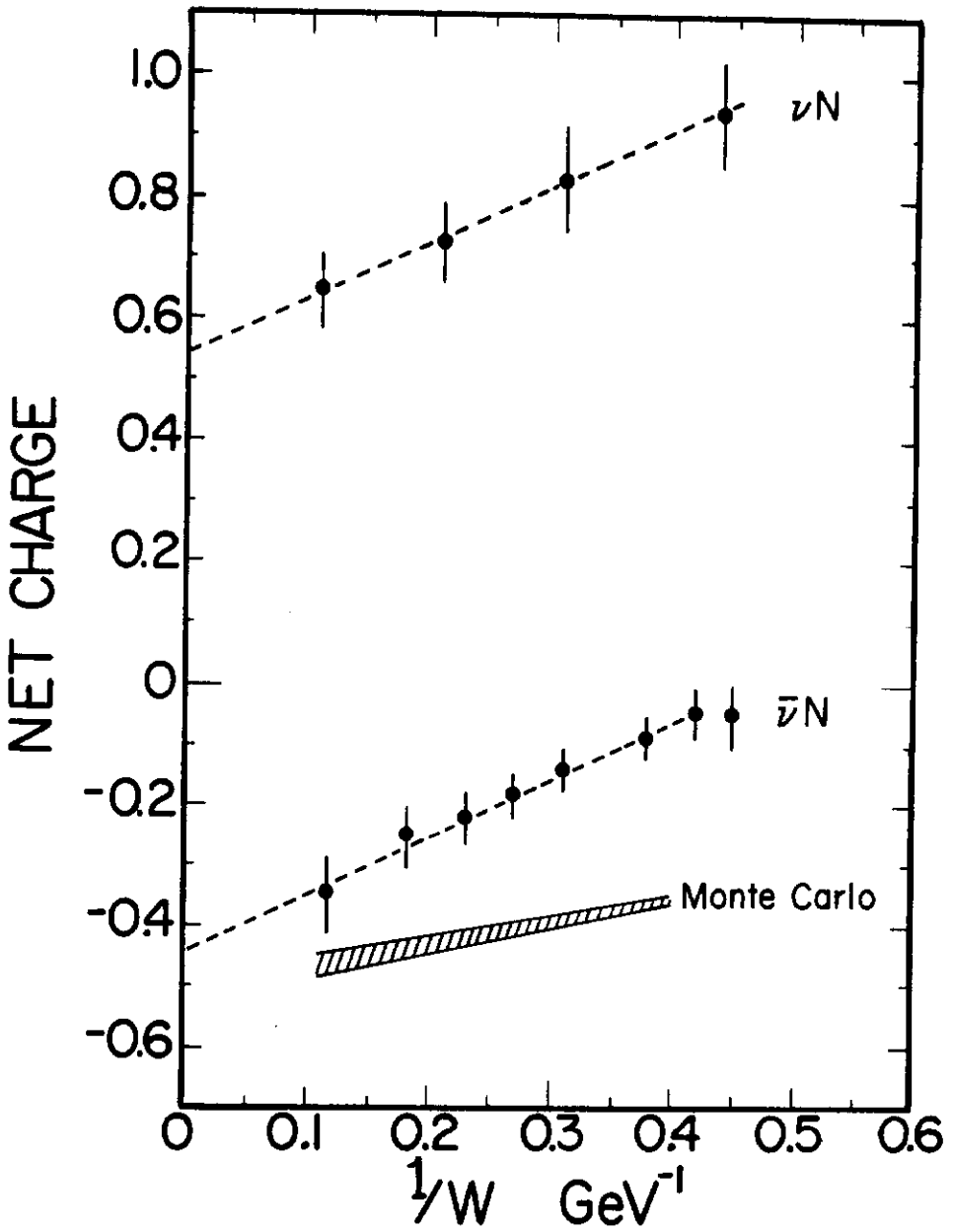
NET CHARGE
1.0
0.8
0.6
0.4
0.2
0
-0.2
-0.4
-0.6
νN
ν̄N
Monte Carlo
0
0.1
0.2
0.3
0.4
0.5
0.6
1/W GeV⁻¹

Fig. 6.

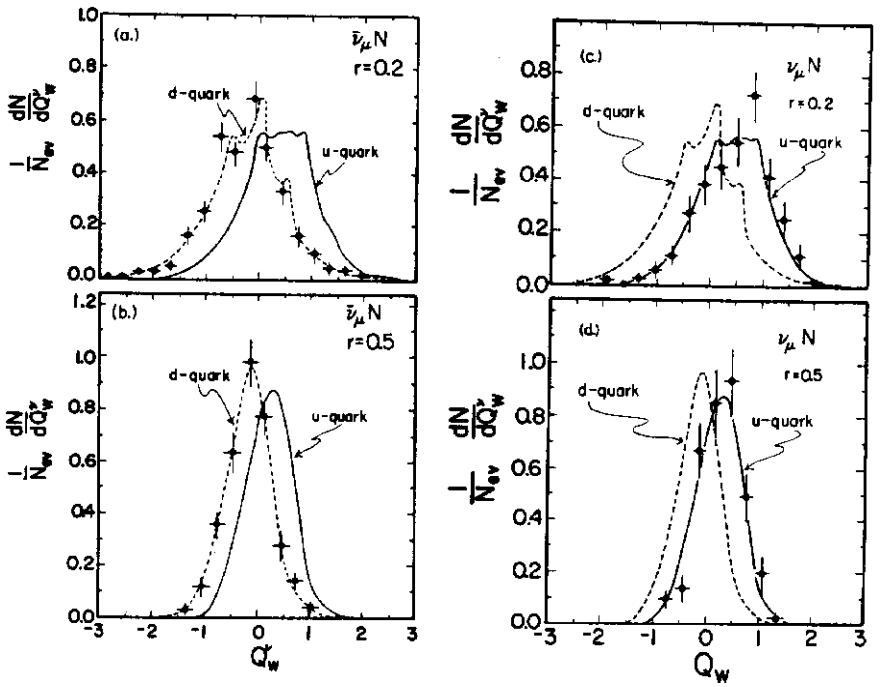
(a.)
$\bar{\nu}_\mu N$
r=0.2
d-quark
u-quark
(b.)
$\bar{\nu}_\mu N$
r=0.5
d-quark
u-quark
(c.)
$\nu_\mu N$
r=0.2
d-quark
u-quark
(d.)
$\nu_\mu N$
r=0.5
d-quark
u-quark
$\frac{1}{N_{cc}}\frac{dN}{dQ_w}$
Q_w

Fig. 7.

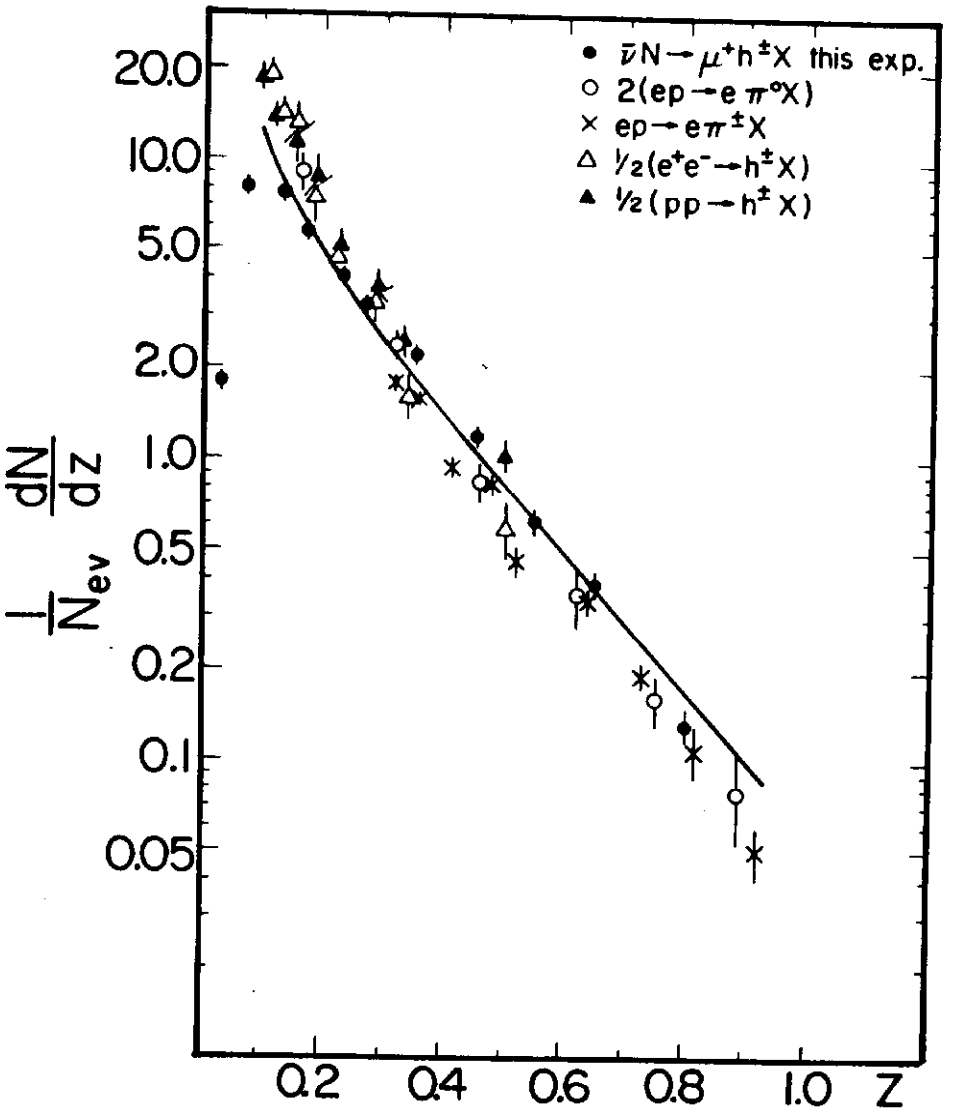
$\bar{\nu}N \to \mu^+ h^\pm X$ this exp.
$2(ep \to e\pi^0 X)$
$ep \to e\pi^\pm X$
$\frac{1}{2}(e^+e^- \to h^\pm X)$
$\frac{1}{2}(pp \to h^\pm X)$
$\frac{1}{N_{ev}} \frac{dN}{dz}$
20.0
10.0
5.0
2.0
1.0
0.5
0.2
0.1
0.05
0.2
0.4
0.6
0.8
1.0
Z

Fig. 8.

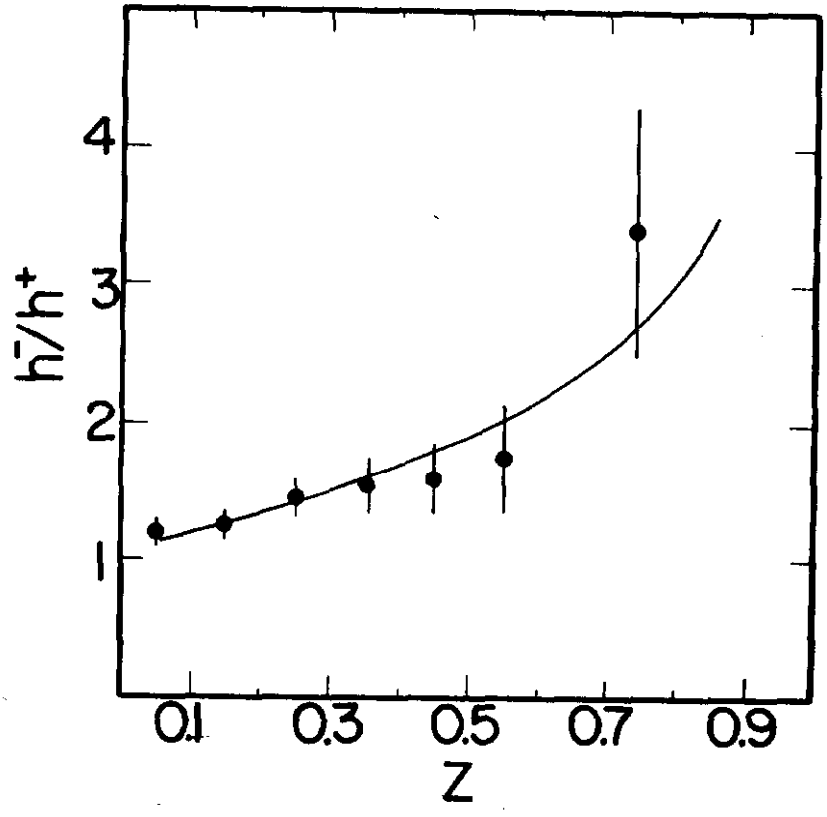

Fig. 9.

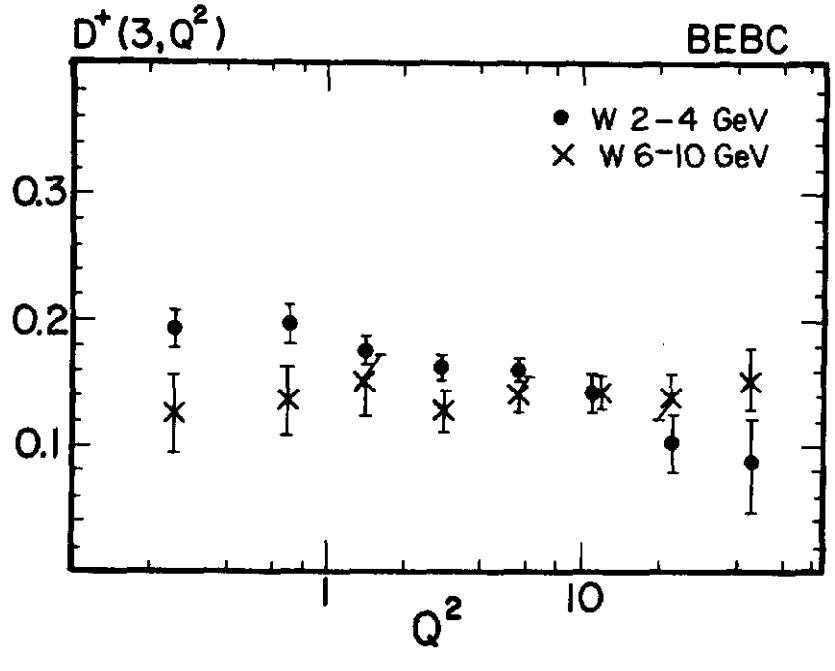

Fig. 10.

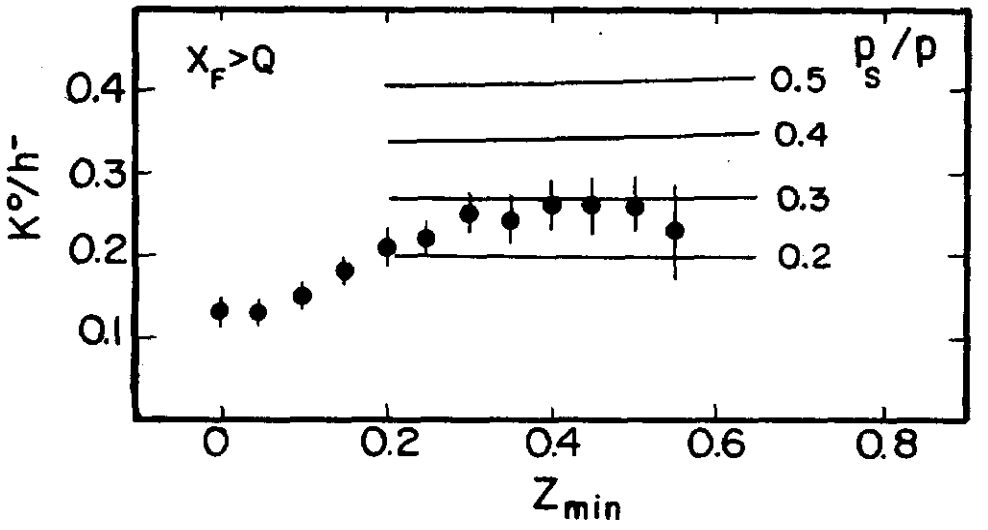

Fig. 11

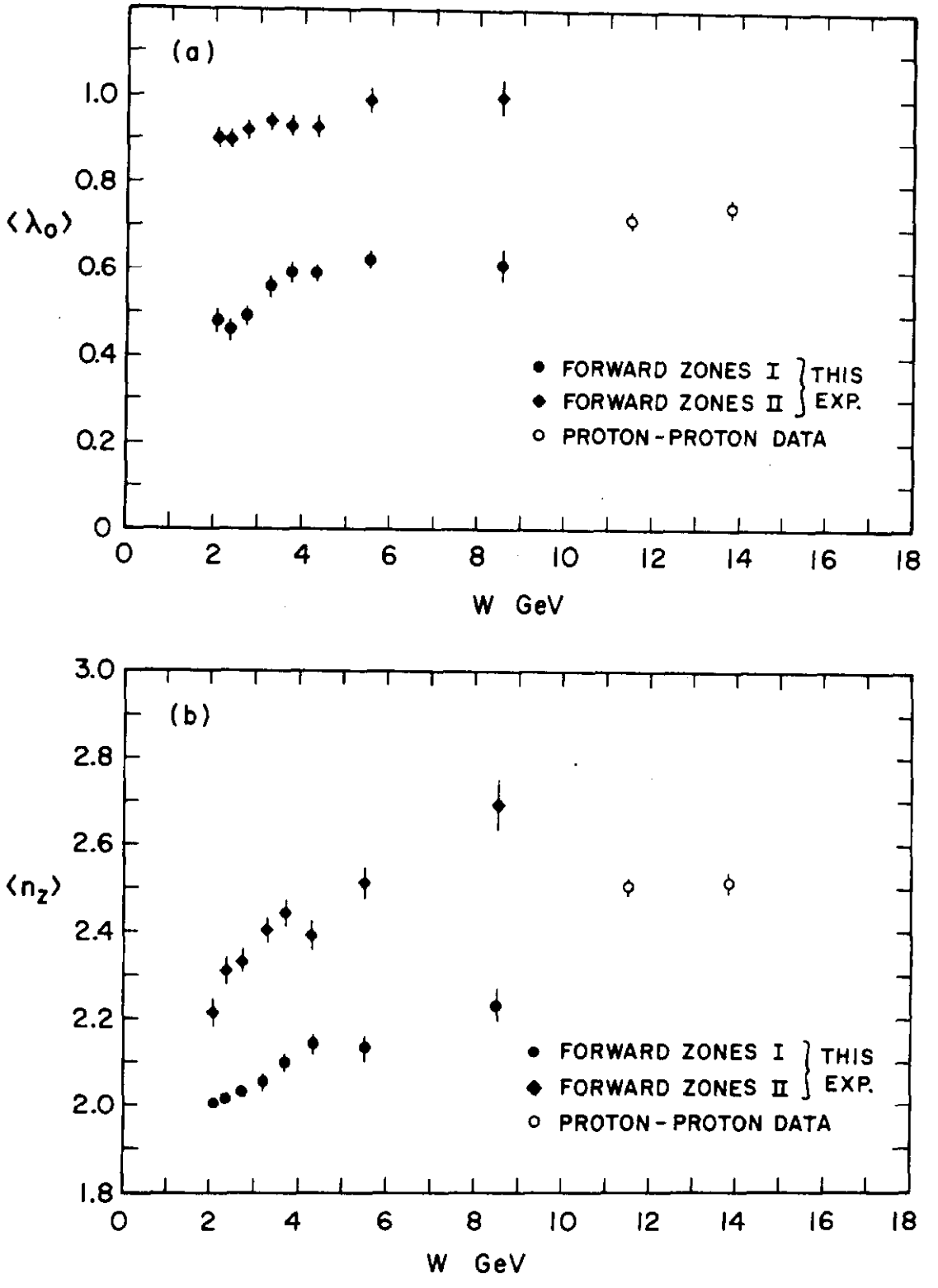
(a)
$\langle \lambda_o \rangle$
1.0
0.8
0.6
0.4
0.2
0
0
2
4
6
8
10
12
14
16
18
W GeV
FORWARD ZONES I
FORWARD ZONES II
THIS EXP.
PROTON-PROTON DATA
(b)
$\langle n_z \rangle$
3.0
2.8
2.6
2.4
2.2
2.0
1.8
0
2
4
6
8
10
12
14
16
18
W GeV
FORWARD ZONES I
FORWARD ZONES II
THIS EXP.
PROTON-PROTON DATA

Fig. 12.

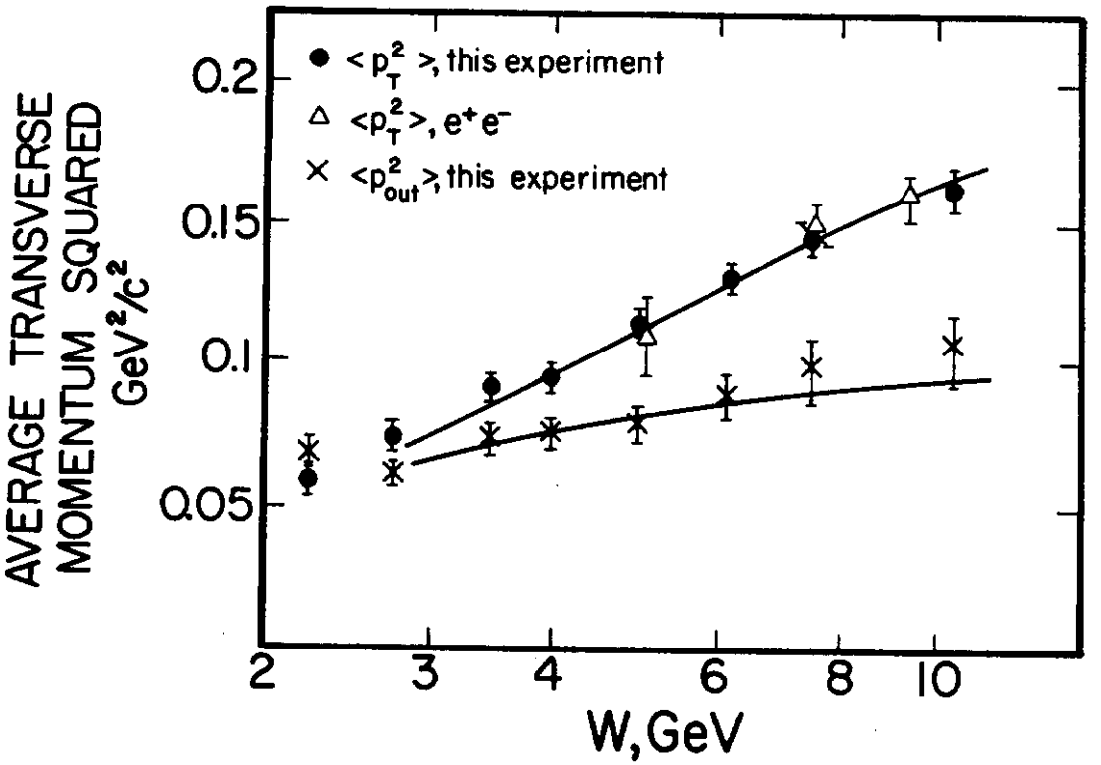
AVERAGE TRANSVERSE MOMENTUM SQUARED GeV²/c²
0.2
0.15
0.1
0.05
● <p²T>, this experiment
△ <p²T>, e⁺e⁻
× <p²out>, this experiment
2
3
4
6
8
10
W, GeV

Fig. 13.